RSC Advances

PAPER

View Article Online
View Journal | View Issue

Cite this: *RSC Adv.*, 2018, **8**, 41850

Enhanced cycling performance of nanostructure $LiFePO_4$/C composites with *in situ* 3D conductive networks for high power Li-ion batteries†

Chunsong Zhao,[a] Lu-Ning Wang,*[ab] Jitao Chen*[c] and Min Gao[d]

Received 4th November 2018
Accepted 22nd November 2018

DOI: 10.1039/c8ra09124b

rsc.li/rsc-advances

In this work, reduced nano-sized $LiFePO_4$ precursor particles were fabricated *via* a green chemistry approach without the use of any organic solvent or surfactants by accelerating the feeding speed of ferrous sulfate. After carbon coating, a 4 nm thick high graphitic degree carbon layer was deposited uniformly on the surface of reduced nano-sized $LiFePO_4$ particles and constructed *in situ* 3D conductive networks among the adjacent $LiFePO_4$ particles, as a result of an elevated self-catalytic effect of the reduced nano-size $LiFePO_4$ particles that promoted the formation of the conductive networks. The reduced nano-size $LiFePO_4$/C particles with *in situ* 3D conductive networks were shown to have an excellent high rate discharge capacity and long cycle life, delivering a high initial reversible discharge capacity of 163 mA h g^{-1} at 0.2C and an even high rate discharge capacity of 104 mA h g^{-1} at 30C. Additionally, a capacity of 101.7 mA h g^{-1} with a capacity retention of 97% remained after 850 cycles at 30C. This work suggests that the enhanced electrochemical performance of the $LiFePO_4$/C composite was improved *via* the combination of the reduced nano-sized and 3D conductive networks, facilitating the electron transfer efficiency and diffusion of lithium ions, especially over an extended cycling performance at a high rate.

Introduction

Since the olivine-type $LiMPO_4$ (M = Fe, Co, Mn, Ni) cathode materials family was successfully explored by Goodenough and co-workers,[1] $LiFePO_4$ has long been considered as a positive electrode material that can be employed as an ideal cathode material for energy storage, electric vehicles (EVs), hybrid EVs, plug-in hybrid EVs and so on, owing to its environmental friendliness, superior cycling lifetime and good thermal stability. Unfortunately, poor electronic conductivity and ionic conductivity[2] seriously hinders its progress for use in practical applications in high performance lithium-ion batteries (LIBs).

To overcome the aforementioned inherent issues of $LiFePO_4$, a variety of approaches have been validated, such as surface coating,[3–8] ionic doping,[9–14] and size and morphology optimization,[15–20] which greatly improved the electronic and ionic conductivity and enhanced its electrochemical performance. One of the conventional methods was used in combination with reduced primary particles and carbon coating to improve the ionic conductivity and electronic conductivity, respectively, for the fabrication of $LiFePO_4$/C composites by solid-state, high-energy ball milling,[21] hydrothermal, solvothermal or supercritical methods.[22,23] However, high-energy ball milling is considered to be less cost-effective, with poor capability and particle morphology control. Zhang *et al.*[24] investigated the effects of ball milling on the properties and electrochemical performance of $LiFePO_4$/C composites and found that a grain size of *c.a.* ~60 nm was obtained from ball milling in acetone with poor morphology and irregular second aggregations, but the composites were capable of delivering an excellent rate capacity of 122 mA h g^{-1} at 10C. As for the hydrothermal (solvothermal) method, besides its high cost facilities, the potential safety risks and harsh operation conditions present problems for its large-scale industrialization. Moreover, the organic solvents used in the filtration process present difficulties and the by-products are hard to recycle, resulting in additional costs for large-scale fabrication, and the chemical oxygen demand (COD) value of the filtrate would be raised due to the use of surfactants.[25] Meanwhile, the introduction of conductive carbon on the surface of $LiFePO_4$ particles through the pyrolysis of solid organic compounds,[26–29] gas phase organic precursors[30,31] and inorganic conductive carbon,[32] significantly accelerates

[a]*Beijing Advanced Innovation Center for Materials Genome Engineering, School of Materials Science and Engineering, University of Science and Technology Beijing, Beijing 100083, China. E-mail: luning.wang@ustb.edu.cn; Tel: +86 10 62332609*

[b]*State Key Laboratory for Advanced Metals and Materials, Beijing 100083, China*

[c]*College of Chemistry and Molecular Engineering, Peking University, Beijing 100871, China. E-mail: chenjitao@pku.edu.cn*

[d]*China Automotive Battery Research Institute Co., Ltd., Beijing 100088, China*

† Electronic supplementary information (ESI) available. See DOI: 10.1039/c8ra09124b

electron migration and improves the electronic conductivity of the material, consequently resulting in an improvement in the reversible insertion and extraction of Li ions and contributes to the high discharge capacity and excellent rate performance of the $LiFePO_4$/C composites. Chen *et al.*[33] reported a strategy to develop excellent kinetics for Li ion insertion and extraction and low cell impedance for $LiFePO_4$ through a carbon coating treatment, hence contributing to an improvement in its high rate capacity. Besides this, the degree of graphitization of the carbon layer on the surface of $LiFePO_4$ particles also has a major effect on the electrochemical performance of the $LiFePO_4$/C composites.[34] The degree of graphitized carbon can be generally measured from a Raman spectrum and the I_D/I_G (disorder/graphite) is closely related to the electronic conductivity of carbon materials.[35,36] As such, a substantial amount of graphitized carbon is essential for the high electronic conductivity of $LiFePO_4$/C composites to promotes the electrode reaction kinetics and enhance the rate performance of the $LiFePO_4$/C cathode material. Nien *et al.*[37] evaluated the electrochemical performance of $LiFePO_4$ composites with different polymer-containing precursors and a better electrochemical performance was observed in the case of a low I_D/I_G value. In order to obtain a high I_D/I_G value for the carbon layer, much attention has been paid to the selection of carbon source precursors,[38] graphitization catalysts,[39–41] carbon preparation method[30,42] and highly graphitic carbon materials[43–45] mixture. Tian *et al.*[46] fabricated a $LiFePO_4$/C composite with a 2–5 nm graphitized carbon thickness by employing a controllable chemical vapor deposition (CVD) approach assisted solid-state route using glucose as a carbon source, which delivered a discharge capacity and voltage of 89.69 mA h g^{-1} and 3.030 V at 200C, respectively. Besides its intrinsic nature, the conductive network also plays a vital role in achieving a continuous electron migration path between adjacent particles and improving the electrical conductivity of $LiFePO_4$/C composites. Such a continuous conductive network favors the diffusion of lithium ions during insertion and extraction, which can be realized by adding inorganic conductive carbon,[43] *in situ* generated[47,48] or through polymer pyrolysis.[49–52] Xu *et al.* [53] constructed an innermost network by *in situ* polymerization of a polyacrylic acid (PAA) layer, adding acetylene black as the second conductive network, and the obtained composites exhibited prominent rate performance and outstanding cycling stability. Although a large number of studies have focused on generating graphitized carbon or conductive networks by introducing catalysts or altering the carbon sources and carbon preparation methods, to date, few studies have focused on the relationships between the graphitized carbon, carbon conductive network and the self-catalytic effects of nano-sized $LiFePO_4$ particles.

Recently, we reported a precipitation approach towards the synthesis of high-performance $LiFePO_4$/C without the need using a hydrothermal (solvothermal) method,[54] the advantages of which are the ability to recycle the filtrate and the zero emission by-products. In this study, nanoscale $LiFePO_4$ particles with a controllable size were successfully precipitated by regulating the feeding rate of a $FeSO_4$ solution without adding any organic solutions or surfactants. Special attention was given to the temperature of the stainless steel reactor, by slightly raising it up to 105 °C from 100 °C to prevent a rapid increase in the viscosity of the slurry as a result of the elevated feeding rate. A uniform carbon coating layer with high quality graphitization was used to cover the surface of $LiFePO_4$ particles with cross-linked conductive carbon between the adjacent $LiFePO_4$ particles to further improve the electron transport and promote the discharge capacity, rate performance, and capacity retention for long cycle life.

Experimental

Preparation of the cathode materials

The details of the fabrication of the precursors were reported in our previous work.[54] Iron(II) sulfate heptahydrate ($FeSO_4 \cdot 7H_2O$, Sinopharm, AR), lithium hydroxide monohydrate ($LiOH \cdot H_2O$, Sinopharm, AR), phosphoric acid (H_3PO_4 (85%), Sinopharm, AR) and deionized water were used in the experiments. In a typical synthesis, 37.8 g of $LiOH \cdot H_2O$ was dissolved in 1.5 L of deionized water and 34.6 g of H_3PO_4 solution was slowly added into the LiOH solution and stirred in a 3 L stainless steel reactor at 55 °C to prepare a Li_3PO_4 suspension. After vigorous stirring for 30 min, 10 g of H_3PO_4 in 100 mL of deionized water was added, and the temperature of the reactor was raised to 105 °C under 20 Pa and the linear velocity of the agitator was set to around 10 m s^{-1} in order to ensure the slurry to be evenly dispersed during the $FeSO_4$ solution addition. Then, 500 mL of deionized water containing 69.5 g of $FeSO_4 \cdot 7H_2O$ was pumped into the boiling Li_3PO_4 suspension over 10 min. The reactor was heated at 105 °C for 5 h, then allowed to naturally cool to room temperature. The resulting product was filtered and washed several times with deionized water and ethanol. Finally, a gray powder was obtained after drying at 80 °C for 12 h in a vacuum oven. The $LiFePO_4$ precursor was labelled as LFP-F. In order to evaluate the effect of different feeding rates of $FeSO_4$ solution on the size and morphology of the $LiFePO_4$ precursor, 200 min of $FeSO_4$ solution feeding was also adopted and the obtained powder was labelled as LFP-S. To synthesize $LiFePO_4$/C, LFP-F and LFP-S were mixed with 7 wt% starch, spray dried and sintered at 700 °C for 8 h under a N_2 atmosphere. The $LiFePO_4$/C composite was obtained and labelled as either LFP/C-F and LFP/

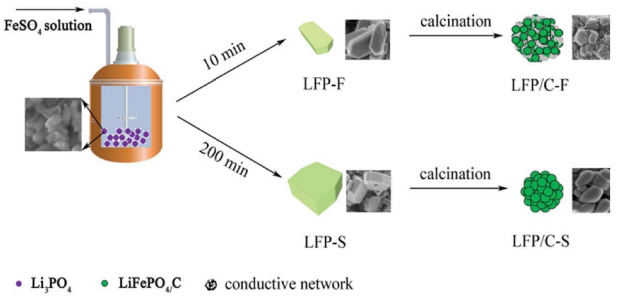

Fig. 1 Schematic representation of the synthesis of $LiFePO_4$/C composites.

C-S. The synthetic process of the $LiFePO_4$ precursor and $LiFePO_4$/C composites is shown in Fig. 1.

Materials characterization

Powder X-ray diffraction (PXRD) analysis of the powdered samples was performed using a Bruker D8-Advantage powder diffractometer with Cu Kα radiation ($\lambda = 1.5405$ Å, 45 kV, 50 mA) between 10° and 80° in reflection geometry mode. The morphology and microstructure of the samples were characterized using a scanning electron microscope (SEM, Sigma 300, ZEISS) equipped with an energy dispersive spectrometer (EDS, Oxford). The carbon coating layer was characterized using a high-resolution transmission electron microscope (HRTEM, JEOL JEM-2010). The carbon layer on the surface of $LiFePO_4$/C was characterized using a Raman spectrometer (Thermo Fisher Scientific, Nicolet Almega XR) and an argon ion laser operating at 632.8 nm. The carbon content of $LiFePO_4$/C was determined using a high-frequency infrared carbon–sulfur analyzer (HCS-800B). The specific surface area was measured by a nitrogen adsorption method using a Brunauer–Emmett–Teller (BET) analyzer (3H-2000PSA2, BeiShiDe Instruments, China). The electronic conductivity of $LiFePO_4$/C composites was measured using a multifunction digital four-probe tester (Suzhou Jingge Electronic Co., Ltd) under 2 MPa.

Electrochemical characterization

The electrochemical performance of the $LiFePO_4$/C materials was measured in CR2032 half coin cells with the $LiFePO_4$/C composites and lithium used as the cathode electrode and counter electrode, respectively. The cathode electrode was fabricated using a mixed slurry of 80 wt% active materials, 10 wt% acetylene black and 10 wt% polyvinylidene fluoride (PVDF) in *N*-methyl pyrrolidone (NMP). Then, the slurry was pasted onto aluminum foil and dried under vacuum at 120 °C for 12 h. The loading of the active materials on the electrode film was kept at around 4.3 mg cm^{-2}, and the electrode film was cut into a circular disc with a diameter of 12 mm. The electrolyte was blended with ethylene carbonate (EC)–dimethyl carbonate (DMC)–ethylmethyl carbonate (EMC) (1/1/1 in volume ratio) dissolved in 1 M $LiPF_6$. Lithium metal plates served as the anode electrodes and Celgard 2400 microporous membrane as the separator. The coin cells were assembled in an argon-filled glove box. Galvanostatic charge–discharge tests were conducted with a Land CT2001 battery tester (Wuhan Land Electronic Co. Ltd., China). Cyclic voltammetry (CV) measurements and electrochemical impedance spectra (EIS) were collected using an electrochemical workstation (CHI 660E). The CV measurements were carried out with different scanning rates at 0.2 mV s^{-1} between 2.0–4.0 V. The EIS measurements were performed over a frequency range of 100 kHz to 10 mHz with an applied amplitude of 5 mV.

Results and discussion

Fig. 2 shows the PXRD patterns of the $LiFePO_4$ precursors and as-synthesized $LiFePO_4$/C composites. It is clear that all of the

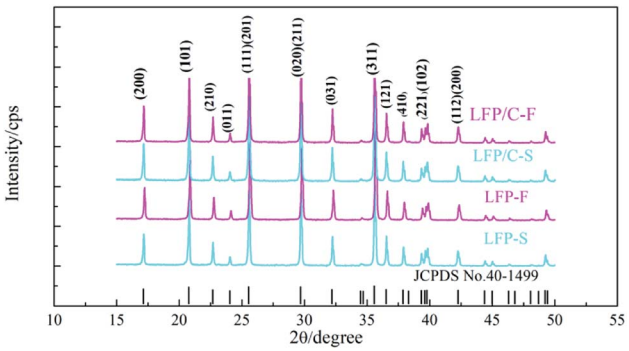

Fig. 2 PXRD patterns of the $LiFePO_4$ precursors and $LiFePO_4$/C composites.

samples are of the $LiFePO_4$ phase with a typical olivine structure indexed by orthorhombic *Pnma*, according to the standard PDF card (JCPDS No. 40-1499), and no impurity phase was detected. The parameters of the lattice parameters and cell volumes of the $LiFePO_4$/C composites were calculated and are shown in Table 1. It can be seen that there are no significant differences between the lattice parameters of the $LiFePO_4$/C composites except that the cell volume of LFP/C-F is slightly smaller.

The crystal sizes of LFP/C-F and LFP/C-S were also calculated using Scherrer's equation ($D = k\lambda/\beta \cos\theta$) in view of the full widths at half maximum (FWHM) of the diffraction peaks [020].[55] It is clear that the crystallite size of LFP/C-F is 61.8 nm, which is smaller than LFP/C-S at 72.5 nm. The decrease in the grain size has the effect of shortening the migration path and increasing the diffusion coefficient for Li ion transport, thus enhancing the electrochemical performance.

The morphologies and particle sizes of the $LiFePO_4$ precursors and $LiFePO_4$/C composites were characterized by SEM, HRTEM and elemental mapping was performed using EDS. As can be seen from the SEM images in Fig. 3a, it is worth noting that the LFP-F micron-sized agglomerated structure grows up to 100 nm in length, with less than 50 nm in width and thickness nanoplates, while that of LFP-S is around 150–200 nm in length and width and 50–100 nm in thickness, as shown in Fig. S1a,† the results of which are due to the nucleation process. According to the crystal nucleation process, a higher reaction concentration generally leads to smaller crystal nucleation. Thus, 50–100 nm of LFP-F precursor was evidently fabricated by shortening the addition time of the $FeSO_4$ solution to 10 min than that of the 150–200 nm of LFP-S precursor at 200 min. Moreover, the smaller ratio of length to width of the LFP-S precursor may be due to the extended reaction process assisted with a modicum of pressure. The LFP/C-F composite presents a second spherical aggregation of 5–10 μm (inset in Fig. 3b)

Table 1 Lattice parameters, cell volumes and crystal sizes of the $LiFePO_4$/C composites

Sample	a (nm)	b (nm)	c (nm)	V (nm^3)	$D_{[020]}$ (nm)
LFP/C-F	1.033	0.6008	0.4695	0.2914	61.8
LFP/C-S	1.034	0.6009	0.4700	0.2920	72.5

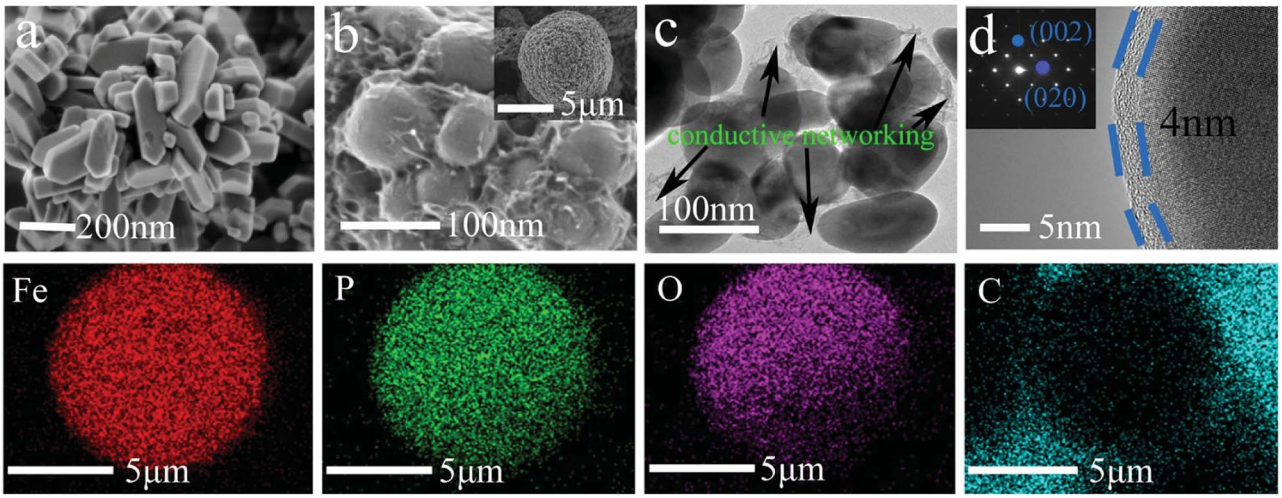

Fig. 3 SEM images of (a) LFP-F and (b) LFP/C-F, TEM images of (c and d) LFP/C-F, and EDS mapping of the Fe, O, P, C elements in the LFP/C-F composite.

and has *c.a.* ~100 nm diameter spherical nano-size particles, caused by volume shrinkage during heat treatment, with a uniform distribution, as shown in Fig. 3b, while the LFP/C-S composite has *c.a.* ~200 nm diameter primary particles with 5–10 μm secondary spherical aggregation, as shown in Fig. S1b.† Moreover, *in situ* grown carbon film frameworks can be seen clearly connecting and entwining the adjacent LFP/C-F particles to form an effective electronic transmission path, which is almost invisible in the LFP/C-S composite. HRTEM images were also acquired to further study the microstructure of the $LiFePO_4$/C composites. The carbon conductive network was obviously observed, as shown in Fig. 3c, with 100 nm nanoparticles and a 4 nm carbon layer was evenly coated on the surface of the LFP/C-F composite, as shown in Fig. 3d. However, few similar conductive networks surround the LFP/C-S particles seen in Fig. S1c† and the thickness of the carbon layer is less than 3 nm on the surface of the LFP/C-S composite shown in Fig. S1d.† The corresponding Fourier filtered transform (FFT) (inset in Fig. 3d) for LFP/C-F exhibits regular spots and further confirms that the $LiFePO_4$ nanoparticles are indeed in a pure crystalline phase.[7] Finally, the elemental mapping results also showed uniform atomic distribution (Fe, P, O and C) for LFP/C-F. According to the BET analysis, the total specific surface areas of the $LiFePO_4$ composites were 24.52 $m^2\ g^{-1}$ and 17.35 $m^2\ g^{-1}$ for LFP/C-F and LFP/C-S, measured from the nitrogen adsorption–desorption isotherms shown in Fig. 4, respectively. The corresponding Barrett–Joyner–Halenda (BJH) pore size distribution curves of the $LiFePO_4$/C composites were also characterized (inset in Fig. 4), and exhibit an average pore diameter of 4.6 nm for the LFP/C-F composite and 3.8 nm for the LFP/C-S, respectively, indicating a similar mesoporous structure for both $LiFePO_4$ composites. Additionally, the carbon content of the LFP/C-F composite was also measured at 2.36 wt%, which is higher than that of the LFP/C-S composite that was measured at a value of 1.94 wt% under the same conditions. The difference in the carbon content may be due to the elevated catalytic effects[56] of the various sized $LiFePO_4$ precursors, resulting in an elevated carbon concentration being generated on the particle surfaces. Thus, the reason for the higher specific surface area of the LFP/C-F composite is due to a higher carbon content, which is favorable for achieving close contact between electrolytes, shortening the lithium ion diffusion path and exhibiting an excellent rate and cycling performance.[57]

It is well known that the degree of graphitization of the surface carbon layer has a significant impact on the electrochemical performance of $LiFePO_4$/C materials.[58] Raman spectroscopy is a common method that can be used to characterize the quality of the carbon layer. Two intense broad bands located at around 1355 cm^{-1} and 1597 cm^{-1} represent the D and G bands[59] of the residual carbon of the LFP/C-F and LFP/C-S composites, respectively, as shown in Fig. 5a and b. In order to analyze the properties of the surface coated carbon, the experimental spectra were fitted using a combination of four Gaussian–Lorentzian bands. The parameters of the band positions, the FWHM and intensities were also refined and are

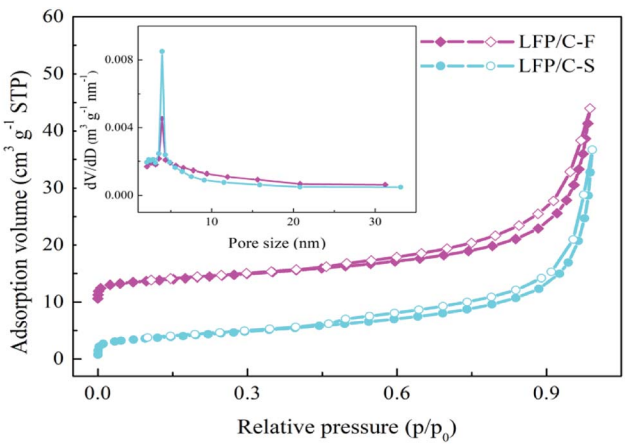

Fig. 4 Nitrogen adsorption/desorption isotherms of the as-prepared LFP/C-F and LFP/C-S composites (inset: pore diameter distribution curves).

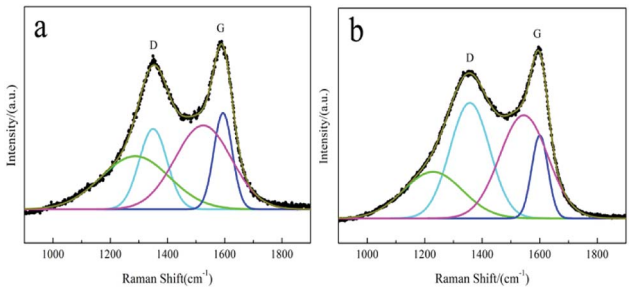

Fig. 5 Raman spectra of the (a) LFP/C-F and (b) LFP/C-S composites.

outlined in Table 2. The D (cyan line) and G (blue line) bands are closely related to the structural and physical properties of the carbon. The other bands at around 1250 cm^{-1} (green line) and 1535 cm^{-1} (magenta line) can be attributed to poorly organized carbon materials and defects outside the planes of the aromatic layers.[34,35] The value of the intensity ratio $R(\lambda_L) = I_D/I_G$ is associated with the nature of the carbon phase.[59] In particular, a graphitic material $R(\lambda_L)$ is related to the in-plane correlation length L_a through a modified Tuinstra–Koenig relationship $L_a = C(\lambda_L)/R(\lambda_L)$, which quantifies the mean basal-plane diameter of graphite parallel to (001) associated with the conductivity. $C(\lambda_L)$ is a variable scaling coefficient correlated to the excitation wavelength (λ_L is 632.8 nm here), and given by $C(\lambda_L) = C_0 + (\lambda_L)C_1$ (ref. 60) with $C_0 = -12.6$ nm and $C_1 = 0.033$. Thus, the value of L_a was 6.41 nm and 2.42 nm for the LFP/C-F and LFP/C-S composites, respectively. It is obvious that the surface carbon layer of the LFP/C-F electrode is more orderly and more graphitized than that of the LFP/C-S electrode, the result of which is consistent with the carbon structure shown in the TEM morphology. As a consequence, the surface carbon of the LFP/C-F composite has a reasonably higher electronic conductivity than that of the LFP/C-S composite, which would be expected to contribute towards the excellent rate and cycling performance of the LFP/C-F composite.

Table 2 Parameters of the D and G bands fitted using the four Gaussian–Lorentzian bands from the spectra of the $LiFePO_4$/C composites

Samples	Parameters		Values
LFP/C-F	Band position (cm^{-1})	D	1350
		G	1594.1
	FWHF (cm^{-1})	D	97.9
		G	64.8
	Intensity (a.u.)	D	166 764.2
		G	132 297.2
	I_D/I_G		1.3
	L_a		6.41
LFP/C-S	Band position (cm^{-1})	D	1357.1
		G	1600.5
	FWHF (cm^{-1})	D	137.9
		G	57.1
	Intensity (a.u.)	D	595 229.5
		G	176 685.2
	I_D/I_G		3.4
	L_a		2.42

The electrochemical performance of the $LiFePO_4$/C cathode materials was evaluated and compared at different current rates from 0.2C to 30C between 2.0 and 4.0 V at 25 °C. Fig. 6a shows the charge and discharge profiles at 0.2C, which is consistent with a two-phase transformation reaction between $FePO_4$ and $LiFePO_4$. The initial discharge capacity of the LFP/C-F electrode was 163 mA h g^{-1}, while that of the LFP/C-S electrode was slightly lower at 158 mA h g^{-1}, resulting from the better reversible performance for Li ion insertion and extraction. The gap between the charge and discharge curves is also presented (inset in Fig. 6a). The mean value of the potential interval (ΔE) of the LFP/C-F composite is 47.4 mV, which is obviously smaller than that at 61.1 mV of the LFP/C-S electrode, suggesting the weaker polarization and more excellent kinetic performance.[61] The rate discharge capacity was evaluated and is compared in Fig. 6b. The discharge specific capacity of the LFP/C-F electrode decreased from 163 mA h g^{-1} to 104 mA h g^{-1} with an increase in the current rate from 0.2C to 30C, while the discharge specific capacity of the LFP/C-S electrode only delivered 157 mA h g^{-1} and 81 mA h g^{-1} under the same test conditions. Besides this, the charge and discharge curves at different rates at current densities from 0.2C to 30C were evaluated for the $LiFePO_4$/C electrodes and the results are shown in Fig. 6c and d. The discharge voltage plateau and capacity gradually decreased upon an increase in the current rates, resulting into electrochemical polarization. However, the relatively low degree of polarization of the LFP/C-F electrode demonstrated the improved kinetics owing to the reduction in particles and higher quality of the coated carbon. Fig. 6e shows the cycling performance of the $LiFePO_4$/C electrodes. The cycling measurements were carried out at room temperature between

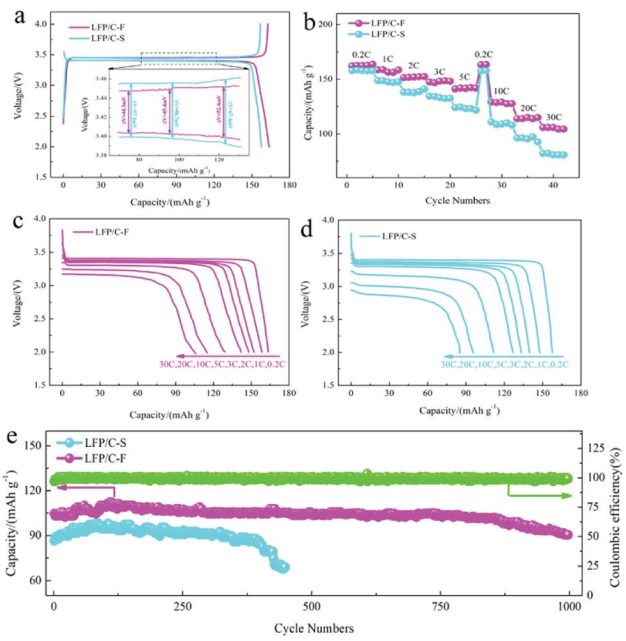

Fig. 6 (a) Galvanostatic cycling profiles of the LFP/C-F and LFP/C-S composites at 0.2C, (b) rate capabilities of the LFP/C-F and LFP/C-S composites at different rates, (c and d) discharge profiles of the LFP/C-F and LFP/C-S composites, and (e) cycling performance of LFP/C-F.

2.0 V and 4.0 V at a rate of 30C. It is obvious that the LFP/C-F electrode delivers a high capacity of 101.7 mA h g^{-1} with a capacity retention of 97% after 850 cycles. In contrast, the LFP/C-S electrode presents an initial capacity of 85 mA h g^{-1} at a rate of 30C. The capacity of the LFP/C-S electrode deteriorated seriously during the cycles and only 50 mA h g^{-1} was retained after 450 cycles. Besides this, the capacity increased over the initial few cycles for both the LFP/C-F and LFP/C-S electrodes, which can be mainly attributed to a gradual increase in the interfacial contact area of the $LiFePO_4$/C electrodes for the electrochemical reaction resulting from the gradual penetration of electrolyte into the interior of the particles, as described in previous literature.[62–64] In other words, the LFP/C-F electrode exhibits more outstanding discharge capacity, rate performance, and cycling performance at a high rate than that of the LFP/C-S electrode, which can be attributed to its reduced particle size and shorter transport path for lithium-ion diffusion through the lattice. Moreover, the combination of the high-quality carbon layer and cross-linked carbon network led to an increase in the conductive interconnection among the adjacent $LiFePO_4$/C particles to form more conductive paths for electrons, which improved the electron transfer efficiency and led to an improvement in the electrochemical performance.

Fig. 7a shows the CV profiles of $LiFePO_4$/C composites at a scan rate of 0.2 mV s^{-1} in the voltage range of 2.0–4.0 V *vs.* Li/Li^+. It can be seen that the cathodic and anodic peak positions of LFP/C-F and LFP/C-S are located at around 3.572 V, 3.654 V and 3.29 V, 3.206 V, respectively, and can be attributed to a Fe^{3+}/Fe^{2+} redox couple. The potential difference (ΔE) between the anodic and cathodic peaks is a key parameter that can be used to examine the reversibility of Li ion insertion and extraction.[65] It is clear that the ΔE value for the LFP/C-F electrode is 0.281 V, which is lower than that of the LFP/C-S electrode at 0.453 V, leading to good reversibility, less polarization and improved kinetics, the results of which are in good agreement with what is shown in the charge and discharge curves. This can be attributed to its reduced particle size and high degree of graphitized carbon on the surface of the LFP/C-F particles with a conductive network between the LFP/C-F particles.

EIS is also an effective method that was used to further evaluate the kinetic reaction of the electrochemical behavior of the $LiFePO_4$/C composites. Fig. 7b shows the Nyquist plots and simulated equivalent circuit, both of which comprise a depressed semicircle at medium frequency and a sloped line at low frequency. The depressed semicircle in the middle frequency region is referred to as the charge transfer resistance (R_{ct}) at the electrolyte/electrode interface and the sloped line in the low frequency region corresponding to the Warburg impedance (Z_w) is related to the diffusion in the bulk of the $LiFePO_4$/C composites.[66] The charge transfer resistance of 10.2 Ω for the LFP/C-F electrode was much lower than that of 16.7 Ω for the LFP/C-S electrode, fitted by the given equivalent circuit (inset in Fig. 7b), illustrating the improved charge transfer kinetics and electronic conductivity due to the higher quality of the carbon layer on the surface of the $LiFePO_4$ particles and compact conductive networks between the $LiFePO_4$ particles. The electronic conductivities of LFP/C-F and LFP/C-S were 8.42 $\times$ 10^{-1} and 2.9 $\times$ 10^{-2} S cm^{-1}, respectively. The results of the EIS indicate that the LFP/C-F electrode has a smaller cell impedance than that of the LFP/C-S electrode, which is consistent with the R_{ct} results. Additionally, the diffusion coefficients (D_{Li}) for the $LiFePO_4$/C composites from the EIS tests can be generally evaluated according to eqn (1):[66]

$$D_{Li} = R^2T^2/2A^2n^2F^4C_0^2\sigma^2 \quad (1)$$

where D_{Li} is the diffusion coefficient in $LiFePO_4$ (cm^2 s^{-1}), R is the gas constant (8.31 J mol^{-1} K^{-1}), T is the absolute temperature (298 K), A is the surface area of the active material, n is the number of electrons transferred per molecule during the electrochemical reaction, F is the Faraday constant (96 485C mol^{-1}), C_0 is the molar concentration of lithium ions in $LiFePO_4$ (1.1 $\times$ 10^{-2} mol cm^{-3} here), and σ is the Warburg factor associated with Z_{re}, calculated using eqn (2):[66]

$$Z_{re} = K + \sigma\omega^{-1/2} \quad (2)$$

The Warburg factor can be obtained from the slope between Z_{re} and $\omega^{-1/2}$ (see Fig. S2†). It can be found from the EIS spectrum that the slope value of the LFP/C-F electrode is less than that of the LFP/C-S electrode, illustrating that the ionic diffusion of the LFP/C-F electrode is more beneficial. The D_{Li} values were calculated to be 6.06 $\times$ 10^{-13} and 2.13 $\times$ 10^{-13} cm^2 s^{-1} for the LFP/C-F and LFP/C-S electrodes, respectively. Therefore, the LFP/C-F electrode exhibits better kinetic behavior, consistent with the above electrochemical performance.

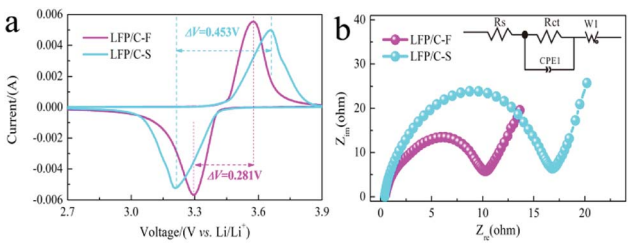

Fig. 7 (a) CV profiles at a scanning rate of 0.2 mV s^{-1} for the LFP/C-F and LFP/C-S composites, and (b) EIS plots in the frequency region of 10^5 to 10^{-2} Hz for the LFP/C-F and LFP/C-S composites (inset: equivalent circuit model).

Conclusions

In this work, $LiFePO_4$ particles with a controllable size were successfully synthesized without the use of any surfactants. The reaction temperature was raised up to 105 °C under 20 Pa pressure in a stainless steel reactor to prevent a soaring in the temperature that would deteriorate the reaction rate. It was found that the size of the $LiFePO_4$ precursor was obviously reduced *via* an increase in the feeding rate of the $FeSO_4$ solution. An elevated self-catalytic effect of nano-sized $LiFePO_4$ particles was observed by SEM, HRTEM and Raman spectroscopy, not only facilitating the formation of a higher quality carbon layer on the surface of the $LiFePO_4$ particles, but also a continuous carbon conductive network was constructed

between the $LiFePO_4$ particles after carbon coating. Beneficially, an initial discharge capacity of the prepared LFP/C-F composite of 163 mA h g^{-1} can be achieved at 0.2C and an even higher rate discharge capacity of 104 mA h g^{-1} at 30C. Moreover, LFP/C-F retains a discharge capacity of 101.7 mA h g^{-1} after 850 cycles at 30C with a capacity retention of 97%. Therefore, the facile size control strategy presented in this study may be a green and effective way to enhance the electron and ion conductivity of $LiFePO_4$ to obtain a high rate and cycling performance.

Conflicts of interest

There are no conflicts to declare.

Acknowledgements

This work was supported by the National Basic Research of China (Grant No. 2015CB932500), the NSF of China (Grant No. 51302141), the National Key Research and Development Program of China (Grant No. 2016YFB0700604) and the Program of the National Natural Science Foundation of China (Grant No. 21673008).

References

1 A. K. Padhi, K. S. Nanjundaswamy and J. B. Goodenough, *J. Electrochem. Soc.*, 1997, **149**, 1188.
2 J. Maier, *Nature*, 2005, **4**, 805.
3 Z. X. Chi, W. Zhang, F. Q. Cheng, J. T. Chen, A. M. Cao and L. J. Wan, *RSC Adv.*, 2014, **4**, 7795.
4 E. Avci, M. Mazman and D. Uzun, *J. Power Sources*, 2013, **240**, 328.
5 P. P. Zhu, Z. Y. Yang, P. Zeng, J. Zhong, J. Yu and J. X. Cai, *RCS Adv.*, 2015, **5**, 107293.
6 L. Dimesso, C. Spanheimer, S. Jacke and W. Jaegermann, *J. Power Sources*, 2011, **196**, 6729.
7 C. S. Zhao, L. N. Wang, H. Wu, J. T. Chen and M. Gao, *Mater. Res. Bull.*, 2018, **97**, 195.
8 J. J. Wang, J. L. Yang, Y. Zhang, Y. L. Li, G. X. Liang, R. Y. Li and X. L. Sun, *Adv. Funct. Mater.*, 2012, **23**, 806.
9 S. Y. Chung and Y. M. Chiang, *Nat. Mater.*, 2002, **1**, 123.
10 J. M. Yang, Y. Bai, C. B. Qing and W. F. Zhang, *J. Alloys Compd.*, 2011, **509**, 9010.
11 F. Lu, Y. C. Zhou, J. Liu and Y. Pan, *Electrochim. Acta*, 2011, **56**, 8833.
12 H. Liu, Q. Cao, L. J. Fu, C. Li, Y. P. Wu and H. Q. Wu, *Electrochem. Commun.*, 2006, **8**, 1553.
13 Z. H. Wang, L. X. Yuan, J. Ma, L. L. Zhang and Y. H. Huang, *Electrochim. Acta*, 2012, **62**, 416.
14 Y. C. Ge, X. D. Yan, J. Liu, X. F. Zhang, J. W. Wang, X. G. He, R. S. Wang and H. M. Xie, *Electrochim. Acta*, 2010, **55**, 5886.
15 X. Q. Ou, H. C. Gu, Y. C. Wu, J. W. Lu and Y. J. Zheng, *Electrochim. Acta*, 2013, **96**, 230.
16 A. V. Murugan, T. Muraliganth and A. Manthiram, *J. Phys. Chem. C*, 2008, **112**, 14665.
17 Y. Y. Liu, J. J. Gu, J. L. Zhang, F. Yu, J. Wang, N. Nie and W. Li, *RSC Adv.*, 2015, **5**, 9745.
18 H. B. Liu, C. Miao, Y. Meng, Y. B. He, Q. Xu, X. H. Zhang and Z. Y. Tang, *Electrochim. Acta*, 2014, **130**, 322.
19 Y. Zhang, W. Wang, P. Li, Y. Fu and X. Ma, *J. Power Sources*, 2012, **210**, 47.
20 N. Recham, L. Dupont and M. Courty, *Chem. Mater.*, 2009, **21**, 1096.
21 J. G. Tu, K. Wu, H. Tang, H. H. Zhou and S. Q. Jiao, *J. Mater. Chem. A*, 2017, **5**, 17021.
22 J. F. Qian, M. Zhou, Y. L. Cao, X. P. Ai and H. X. Yang, *J. Phys. Chem. C*, 2010, **114**, 3477.
23 S. A. Hong, S. J. Kim, J. Kim, K. Y. Chung, B. W. Cho and J. W. Kang, *Res. Chem. Intermed.*, 2011, **37**, 429.
24 D. Zhang, R. Cai, Y. K. Zhou, Z. P. Shao, X. Z. Liao and Z. F. Ma, *Electrochim. Acta*, 2010, **55**, 2653.
25 B. Pei, H. Yao, W. Zhang and Z. Yang, *J. Power Sources*, 2012, **220**, 317.
26 H. Huang, S. C. Yin and L. F. Nazar, *Electrochem. Solid-State Lett.*, 2001, **4**, A170.
27 H. Gabrisch, J. D. Wilcox and M. M. Doeff, *Solid-State Lett.*, 2006, **9**, A360.
28 Y. Lin, M. X. Gao, D. Zhu, Y. F. Liu and H. G. Pan, *J. Power Sources*, 2008, **184**, 444.
29 R. Dominko, M. Bele, M. Gaberscek, M. Remskar, D. Hanzel, S. Pejovnik and J. Jamnik, *J. Electrochem. Soc.*, 2005, **152**, A607.
30 W. L. Shang, L. Y. Kong and X. W. Ji, *Solid State Sci.*, 2014, **38**, 79.
31 K. Amine, J. Liu and I. Belharouak, *Electrochem. Commun.*, 2005, **7**, 669.
32 K. Zaghib, J. Shim, A. Guerfi, P. Charest and K. A. Striebel, *Electrochem. Solid-State Lett.*, 2005, **8**, A207.
33 J. M. Chen, C. H. Hsu, Y. R. Lin, M. H. Hsiao and G. T. K. Fey, *J. Power Sources*, 2008, **184**, 498.
34 Y. Q. Hu, M. M. Doeff, R. Kostecki and R. Finones, *J. Electrochem. Soc.*, 2004, **151**, A1279.
35 M. M. Doeff, Y. Q. Hu, F. McLarnon and R. Kostecki, *Electrochem. Solid-State Lett.*, 2003, **6**, A207.
36 J. D. Wilcox, M. M. Doeff, M. Marcinek and R. Kostecki, *J. Electrochem. Soc.*, 2007, **154**, A389.
37 Y. H. Nien, J. R. Carey and J. S. Chen, *J. Power Sources*, 2009, **193**, 822.
38 J. K. Kim, J. W. Choi, G. S. Chauhan, J. H. Ahn, G. C. Hwang, J. B. Choi and H. J. Ahn, *Electrochim. Acta*, 2008, **53**, 8258.
39 T. Nakamura, Y. Miwa, M. Tabuchi and Y. Yamada, *J. Electrochem. Soc.*, 2006, **153**, A1108.
40 C. W. Ong, Y. K. Lin and J. S. Chen, *J. Electrochem. Soc.*, 2007, **154**, A527.
41 X. H. Yang, Y. Y. Mi, W. D. Zhang, B. R. Wu and H. H. Zhou, *J. Power Sources*, 2015, **275**, 823.
42 B. Zhao, Y. Jiang, H. Zhang, H. Tao, M. Zhong and Z. Jiao, *J. Power Sources*, 2009, **189**, 462.
43 W. Liu, P. Gao, Y. Y. Mi, J. T. Chen, H. H. Zhou and X. X. Zhang, *J. Mater. Chem. A*, 2013, **1**, 2411.
44 F. Y. Su, C. You, Y. B. He, W. Lv, W. Cui, F. Jin, B. Li, Q. H. Yang and F. Y. Kang, *J. Mater. Chem.*, 2010, **20**, 9644.
45 M. S. Bhuvaneswari, N. N. Bramnik, D. Ensling, H. Ehrenberg and W. Jaegermann, *J. Power Sources*, 2008, **180**, 553.

46 R. Y. Tian, H. Q. Liu, Y. Jiang, J. K. Chen, X. H. Tan, G. Y. Liu, L. N. Zhang, X. H. Gu, Y. J. Guo, H. F. Wang, L. F. Sun and W. G. Chu, *ACS Appl. Mater. Interfaces*, 2015, **7**, 11377.
47 J. L. Yang, J. J. Wang, Y. J. Tang, D. N. Wang, B. W. Xiao, X. F. Li, R. Y. Li, G. X. Liang, T. K. Sham and X. L. Sun, *J. Mater. Chem. A*, 2013, **1**, 7306.
48 C. Y. Wu, G. S. Cao, H. M. Yu, J. Xie and X. B. Zhao, *J. Phys. Chem. C*, 2011, **115**, 23090.
49 Y. Y. Xing, Y. B. He, B. H. Li, X. D. Chu, H. Z. Chen, J. Ma, H. D. Du and F. Y. Kang, *Electrochim. Acta*, 2013, **109**, 512.
50 W. J. Ren, K. Wang, J. L. Yang, R. Tan, J. T. Hu, H. Guo, Y. D. Duan, J. X. Zheng, Y. Lin and F. Pan, *J. Power Sources*, 2016, **331**, 232.
51 B. S. Lalia, T. Shah and R. Hashaikeh, *J. Power Sources*, 2015, **278**, 314.
52 Y. F. Tang, F. Q. Huang, H. Bi, Z. Q. Liu and D. Y. Wan, *J. Power Sources*, 2012, **203**, 130.
53 D. W. Xu, X. D. Chu, Y. B. He, Z. J. Ding, B. H. Li, W. J. Han, H. D. Du and F. Y. Kang, *Electrochim. Acta*, 2015, **152**, 398.
54 C. S. Zhao, L. N. Wang, J. T. Chen and M. Gao, *Electrochim. Acta*, 2017, **255**, 266.
55 Y. Y. Liu, J. J. Gu, J. L. Zhang, J. Wang, N. Nie, Y. Fu, W. Li and F. Yu, *Electrochim. Acta*, 2015, **173**, 448.
56 J. J. Wang, J. L. Yang, Y. J. Tang, J. Liu, Y. Zhang, G. X. Liang, M. Gauthier, X. F. Li, R. Y. Li, J. Wang, T. K. Sham and X. L. Sun, *Nat. Commun.*, 2014, **5**, 3415.
57 J. L. Yang, J. J. Wang, D. N. Wang, X. F. Li, D. S. Geng, G. X. Liang, M. Gauthier, R. Y. Li and X. L. Sun, *J. Power Sources*, 2012, **208**, 340.
58 B. Wang, T. F. Liu, A. M. Liu, G. J. Liu, L. Wang, T. T. Gao, D. L. Wang and X. S. Zhao, *Adv. Energy Mater.*, 2016, **6**, 1600426.
59 M. Maccario, L. Croguennec, B. Desbat, M. Couzi, F. Le Cras and L. Servant, *J. Electrochem. Soc.*, 2008, **155**, A879.
60 M. J. Matthews, M. A. Pimenta, G. Dreesselhaus, M. S. Dreesselhaus and M. Endo, *Phys. Rev. B*, 1999, **59**, R6585.
61 M. M. Chen, Q. Q. Ma, C. Y. Wang, X. Sun, L. Q. Wang and C. Zhang, *J. Power Sources*, 2014, **263**, 268.
62 R. Dominko, J. M. Goupil, M. Bele, M. Gaberscek, M. Remskar, D. Hanzel and J. Jamnik, *J. Electrochem. Soc.*, 2005, **152**, A858.
63 R. Dominko, M. Bele, M. Gaberscek, M. Remskar, D. Hanzel, J. M. Goupil, S. Pejovnik and J. Jamnik, *J. Power Sources*, 2006, **153**, 274.
64 X. L. Wu, L. Y. Jiang, F. F. Cao, Y. G. Guo and L. J. Wan, *Adv. Mater.*, 2009, **21**, 2710.
65 C. Su, X. D. Bu, L. H. Xu, J. L. Liu and C. Zhang, *Electrochim. Acta*, 2012, **64**, 190.
66 S. W. Oh, Z. D. Huang, B. Zhang, Y. Yu, Y. B. He and J. K. Kim, *J. Mater. Chem.*, 2012, **22**, 17215.